Peer Review File

Manuscript Title: A dynamically reprogrammable metasurface with self-evolving shape morphing

Reviewer Comments & Author Rebuttals

Reviewer Reports on the Initial Version:

Referee expertise:

Referee #1: soft materials actuation

Referee #2: design automation and programmable matter

Referees' comments:

Referee #1 (Remarks to the Author):

This work introduces a clever way of morphing a flexible sheet using Lorentz forces acting on a grid of embedded programmable wires. This flexible sheet is placed in a very large static magnetic field created by two surrounding magnets, and the current distribution modulated to dynamically morph the sheet. The results are quite interesting, and the capability is clearly demonstrated, perhaps best seen in the videos. This difficult problem is studied in depth, with convincing theoretical/algorithmic results and several interesting demonstrations.
Such dynamic (reprogrammable) deformation is indeed difficult to achieve with most shape morphing schemes. I see this work as being of interest to

This method of sheet morphing is rather unique from other methods, due to the fact that the deformation force acts on the sheet from an external source, rather than being due to internal stress. This is one factor enabling large deformations, relatively fast speed and some level of complexity in achieved shapes.

The modelling and control approach taken here is strong and shows excellent performance. The model-based optimization process works great although it would be computationally expensive for more complex shapes which may require a non-linear model. The sensor-feedback closed loop control method is impressive to handle such cases and the potential for model-free control is great.

I have seen a similar mode of actuation used in different geometric forms, for example the use of embedded wires in steerable catheters operating inside an MRI machine. Although I am not aware of any sheet-like morphing examples using this method, I find it a problem that no prior work is cited in the area of Lorentz-driven flexible devices more generally.
As just one latest example: https://doi.org/10.1002/advs.202105352

A clear downside of this method is that the field strength used must be very large. It may be difficult to generate such 0.225 T fields over a larger distance for application. That being said, the trace currents (maximum of 27.5 mA) are reasonable.

I don’t know if I would call it “self-morphing” since the morphing is induced by external controls.

Referee #2 (Remarks to the Author):

This manuscript proposes a novel metasurface that can dynamically morph its shape by having reprogrammable, distributed Lorentz forces. The proposed metasurface is made up by a mesh of serpentine-shaped beams, and desired Lorentz forces can be generated by controlling the electrical current across the beams under a static magnetic field (~0.2 T). There are two control schemes for the proposed metasurface – the open-loop, model-based actuation method and the closed-loop, experiment-driven actuation method. Some notable features of the proposed metasurface are that it can generate a wide range of 3D shapes with high precision and speed (~0.1 s), and it is also very robust since it can still morph into the desired shapes despite having extrinsic or intrinsic perturbations. Such abilities are unprecedented and I believe that the proposed metasurface is highly desirable across a broad range of applications pertaining to soft robotics, wearable technologies and advanced materials.

Overall, I think that this is an excellent novel work, which demonstrates a significant advancement for shape-(re)programmable soft matter. The manuscript is well-written and there is also sufficient data to support the conclusion of this work. The presented showcases are very impressive too. Here are some suggestions that I hope will be beneficial for the authors:

1. I believe that the range of shapes which can be generated by the proposed metasurface is dependent on its number of independent input voltages. Specifically, a larger range of shapes should be achievable when there are more independent input voltages for the metasurface. In view of this point, can the authors discuss what is the maximum number of voltage inputs that they can provide for their proposed metasurface based on manufacturing or other constraints? Is it possible to create metasurfaces that have more input voltages than the presented 2x2, 4x4 and 8x8 samples in the future?

2. Similar to Point #1, I believe that the range of shapes that can be generated by the metasurface is also dependent on the applied magnetic field. In this study, the applied magnetic field is static and assumed to be uniform due to the configuration of the external magnets. Will it be possible to enhance the range of producible shapes by introducing non-uniform magnetic fields that can also vary with respect to time? I believe that the manuscript can be further strengthened if such discussions can be added.

3. While the proposed metasurface is able to dynamically generate a wide range of shapes, beam bending seems to be its dominant mode of deformation, and I did not observe large tensile or compressive deformations in the experiments. Based on this discussion, I believe that it will be good to explicitly discuss about the available modes of deformation of the proposed metasurface in the manuscript.

4. For both the open-loop and the closed-loop actuation methods, a gradient-based algorithm is used to solve an optimization problem that minimizes the error of the system. Are these convex optimization problems? If so, I think that it will be good to state this explicitly in the manuscript as this means that the obtained solution will always be the global solution. If they are not convex optimizations, can the authors discuss about the possibility of getting trapped in a local solution? Although global solvers such as the evolutionary algorithms or particle swarm algorithms are slower than their gradient-based counterparts, will they be helpful in such scenarios?

Guo Zhan Lum

[Redacted]

1. discussion of related previous work and limitations (Reviewer #1)

Our response: We expanded our discussion and added additional references to related previous work utilizing programmable stimuli to enable shape shifting, with a focus on Lorentz-force-driven flexible devices more generally. While several recent works demonstrate actuators that can switch between fixed shapes, no continuously, dynamically reprogrammable shape morphing systems have been reported before. In addition to the basic notion and overall architecture of a mesh of optimized, planar serpentine conductive features, a key advance in our work lies in the inverse design of nonlinear systems. For soft morphing matter driven by distributed stimuli, the input-output relation (especially in the regime of large deformation that is necessary for shape morphing) is usually highly nonlinear, leading to difficulties in finding the desired inputs (*e.g.*, electric currents or voltages) such that the precursor structure can deform into the target shapes, *i.e.,* the inverse problem. Our work provides two ways to address this challenge: (1) we designed an approximately linear input-output soft morphing system with easily accessible solutions to the inverse problem, (2) we invented a model-free, experiment-driven solution when the system deviates from the linear, time-invariant response. We added text to highlight the fundamental limitations in the accessible design space and the intrinsic difficulties of these previous works.

In terms of limitations, we outlined several engineering pathways to deploy our systems in magnetic fields with significantly lower strength to enable applications over a larger distance, as the electromagnetic response of the serpentine beams is widely tunable following the scaling law (Extended Data Fig. 2) to enable the same morphing capability in small-strength fields. Our systematic studies of the Lorentz-force-driven metasurface allow for optimized choices of geometries, layouts, materials, and digital-physical interface (voltage/current supply, magnetic field strength) for a large range of application requirements. We added Extended Data Fig. 2 to provide additional experiments to validate the scaling law. We included detailed discussions in Supplementary Notes S3 and S5.

Modification to the manuscript: On page 3, line 57, we modified the text to the following "The desire to shift shapes among a number of configurations invites investigations of various architectures and programmable stimuli (*e.g.,* temperature[13,42], magnetic field[20,43], electric field[14], Lorentz-force actuation[22,23,44]). A materials architecture that consists of a mesh of optimized, planar serpentine conductive features operating in a magnetic field and with programmable control over distributions of electrical current, as introduced here, presents an intriguing set of opportunities. Traditional inverse design of the input-output relationships in the resulting nonlinear and high-dimensional system can, however, leading to difficulties in establishing analytical

solutions or problems in high computational costs." We included the 1-dimensional example suggested by the referee (Ref. 44 in the revised manuscript), as well as additional sheet-like shape-shifting example based on electric-field driven dielectric elastomers (Ref. 14 in the revised manuscript), to cover prior work in this area more generally. We removed less relevant references (Refs. 14*, 39* and 41* in the original manuscript) to meet the editorial policy on total number of references.

On page 10, line 232, we added and revised the text to highlight the addressed challenges "The Lorentz-force-driven serpentine mesh construction supports an approximately linear input-output response with easily accessible solutions to the inverse problem. The highly integrable digital-physical interfaces incorporating actuation, sensing, and feedback allow for an in-loop optimization process to attain model-free, experiment-driven solutions when the system deviates from the linear, time-invariant response. The resulting metasurface can follow a self-evolving inverse design to morph to target shapes without prior knowledge of physics, or with a model-driven prediction to expedite the evolving process."

On page 5 of the Supplementary Information, in Supplementary Note S3.1, we added a detailed discussion of the design principles.

On page 9 of Supplementary Information, in Supplementary Note S5.1, we added the text to present the experimental validation of the scaling law.

We added Extended Data Fig. 2 in the revised manuscript.

Please refer to our responses to comments of Referee #1 for more details.

2. and **additional clarifications and discussion regarding the parameters around the shape morphing (Reviewer #2)**

Our response: We expanded our discussion of the achievable range of shapes supported by our system, with a focus on the effect of the number of independent voltage control ports and the presence of non-uniform magnetic fields that can also vary with respect to time, following Reviewer #2's suggestion. We added text in the revised manuscript to provide principal design guidelines to tailor the parameters for specific shape morphing requirements in the future. We performed additional experiments and FEA to showcase the enhancement of the shape-morphing range upon the introduction of time-variable non-uniform magnetic fields.

We provided a discussion regarding the convexity of our optimization problems and investigated the limitations of a gradient-based solver in the experiment-driven process. We also explored global optimization methods as an alternative approach.

Modification to the manuscript: On page 6, line 134, we added a summary of the suggested ways to enhance the range of shapes, as follows "Increasing the number of control inputs and introducing time-varying magnetic fields and field gradients greatly enhance the range of target shapes that can be realized (see Extended Data Fig. 3, Supplementary Figs. 28 and 29, and Supplementary Notes S7 and S12)." We referred the detailed discussions to Supplementary Information.

On page 14 of the Supplementary Information, we added Supplementary Note S7 to discuss the approaches to increase the number of voltage inputs.

We added Extended Data Fig. 3, Supplementary Fig. 29, and Supplementary Note S12 to discuss the deformation in a non-uniform magnetic field.

On page 2 of the Supplementary Information, in Supplementary Note S2.1, we added text to describe the simulation of non-uniform magnetic fields.

We added Ref. 43 to refer to methods to generate time-varying, non-uniform magnetic fields.

On Page 4, line 80, we added the text "A tailored serpentine design ensures sufficiently large, fast, and reversible out-of-plane deformation ($u/L \sim 30\%$; in-plane deformation <0.01L; response time <0.07 s) of the serpentine beam …" to discuss the mode of deformation in our system.

On page 11, line 256, we added the text to discuss ways to achieve additional modes of deformation for future study "Exploring constructions with low in-plane stiffness will enable additional deformation modes of the metasurface (see Supplementary Fig. 34)."

We included Supplementary Fig. 34 to show the illustration of appreciable in-plane deformation realized in the proposed system with low in-plane stiffness.

On pager 12, 13 of the Supplementary Information, in Supplementary Note S6.2, we added text to discuss the convexity of our optimization problems and explored global solvers as an alternative approach.

Please refer to our responses to comments of Referee #2 for more details.

We will need to consider your response to these concerns in the form of a revised manuscript accompanied by a list to explain your revisions.

Our response: Thank you for providing us with the opportunity to revise the manuscript and considering its publication in *Nature*. We are pleased to know that the referees found our research interesting. We are grateful for their comments and suggestions and we have carefully addressed all of them in the revised manuscript.

Modification to the manuscript: We selected and reorganized ten Extended Data Figures following the main figures. Extended Data Figs. 2, 3, 4d–f, are newly added from this revision. The remaining comes from Supplementary Figs. 2, 4, 30, 31, 32, 36, 37, 38, and 39 in the original manuscript.

In Fig. 1a, we added a space between the numerical value and unit symbol. We modified the labels in Figs. 1b, c.

On Page 16, we added entities and people to acknowledge "This work was performed in part at the Duke University Shared Materials Instrumentation Facility (SMIF), a member of the North Carolina Research Triangle Nanotechnology Network (RTNN), which is supported by the National Science Foundation (award number ECCS-2025064) as part of the National Nanotechnology Coordinated Infrastructure (NNCI). Xiaoyue Ni thanks Leila Bridgeman, Jianfeng Lu, and Zhaoran Wang for helpful discussions."

We modified Supplementary Video 4 to avoid duplication of information already shown in the main figure, providing more examples of morphing process via experiment-driven process. We modified the legends accordingly. We improved the quality of Video 8.

Responses to comments of Referee #1

Comments from Referee #1:

Summary Comment: This work introduces a clever way of morphing a flexible sheet using Lorentz forces acting on a grid of embedded programmable wires. This flexible sheet is placed in a very large static magnetic field created by two surrounding magnets, and the current distribution modulated to dynamically morph the sheet. The results are quite interesting, and the capability is clearly demonstrated, perhaps best seen in the videos. This difficult problem is studied in depth, with convincing theoretical/algorithmic results and several interesting demonstrations.

Such dynamic (reprogrammable) deformation is indeed difficult to achieve with most shape morphing schemes. I see this work as being of interest to

This method of sheet morphing is rather unique from other methods, due to the fact that the deformation force acts on the sheet from an external source, rather than being due to internal stress. This is one factor enabling large deformations, relatively fast speed and some level of complexity in achieved shapes.

The modelling and control approach taken here is strong and shows excellent performance. The model-based optimization process works great although it would be computationally expensive for more complex shapes which may require a non-linear model. The sensor-feedback closed loop control method is impressive to handle such cases and the potential for model-free control is great.

Our response: We thank the referee for these insightful and positive comments. We included additional discussions, simulations, and experimental results in the revised manuscript to address the referee's comments listed below.

Modification to the manuscript: None.

Comment 1: I have seen a similar mode of actuation used in different geometric forms, for example the use of embedded wires in steerable catheters operating inside an MRI machine. Although I am not aware of any sheet-like morphing examples using this method, I find it a problem that no prior work is cited in the area of Lorentz-driven flexible devices more generally. As just one latest example: https://doi.org/10.1002/advs.202105352

Our response: We thank the referee for this comment. We agree that Lorentz force has been reported in literature as a mode of actuation. Our original manuscript cited two papers on Lorentz-force-driven flexible devices where we discussed programmable stimuli based on electric current (Refs. 22 and 23 in the revised manuscript). We found these references to be most relevant to our work as they bear some resemblance to shape-shifting sheets.

[22] Mao, G. *et al., Sci. Adv.* **6**, eabc0251 (2020).
[23] Zhang, F. *et al.*, *Proc. Natl. Acad. Sci. U.S.A.* **118**, e2026414118 (2021).

In the revised manuscript, we explicitly use "Lorentz-force actuation" instead of "electric current" for clarity. We included the 1-dimensional example suggested by the referee (Ref. 44 in

the revised manuscript), as well as additional sheet-like shape-shifting example based on electric-field driven dielectric elastomers (Ref. 14 in the revised manuscript), to cover prior work in this area more generally. We removed less relevant references (Refs. 14*, 39* and 41* in the original manuscript) to meet the editorial policy on total number of references:

[14] Hajiesmaili, E. & Clarke, D. R., *Nat. Commun.* **10**, 183 (2019).
[44] Phelan III, M. F., *et al.*, Adv. Sci., 2105352 (2022, Early View).
[14*] Kotikian, A. *et al.*, *Adv. Mater.* **30**, 1706164 (2018).
[39*] Yao, Y. *et al.*, *Proc. Natl. Acad. Sci. U.S.A.* **115**, 12950 – 12955 (2018).
[41*] Park, J. K. *et al.*, *Adv. Mater.* **31**, 1905715 (2019).

Our modifications to the manuscript: On page 3, line 57, we modified the text to "The desire to shift shapes among a number of configurations invites investigations of various architectures and programmable stimuli (*e.g.,* temperature[13,42], magnetic field[20,43], electric field[14], Lorentz-force actuation[22,23,44]). A materials architecture that consists of a mesh of optimized, planar serpentine conductive features operating in a magnetic field and with programmable control over distributions of electrical current, as introduced here, presents an intriguing set of opportunities. Traditional inverse design of the input-output relationships in the resulting nonlinear and high-dimensional system can, however, leading to difficulties in establishing analytical solutions or problems in high computational costs."

On page 3, line 51, we modified the text to "Smart materials (*e.g.,* liquid crystal elastomers[11,13,15–17,39], dielectric elastomers[14], responsive hydrogels[10,12,24], and others[25]) and multimaterial structures[11,26] enable large structural deformation but face challenges in implementing fast control to refined structures."

We removed Refs. 14*, 39* and 41* in the original manuscript and added Refs. 14 and 44 in the revised manuscript.

Comment 2: A clear downside of this method is that the field strength used must be very large. It may be difficult to generate such 0.225 T fields over a larger distance for application. That being said, the trace currents (maximum of 27.5 mA) are reasonable.

Our response: We thank the referee for this comment. While a large magnetic field B is beneficial for large actuation output using minimal currents and low energy consumption, we agree with the referee that a smaller magnetic field is preferred in some applications over larger distances. The analytical model and scaling law presented in the manuscript (Page 4, line 80 and page 5, line 102) and Supplementary Notes S3 and S4 establish guidelines in explicit forms for the design of systems with the same morphing capability but in fields with small strength.

We provided additional experimental characterization of the tunable electromagnetic response of serpentine beams with various widths (H = 0.84 mm, 1.20 mm, 1.56 mm) and thicknesses (h_{PI} = 5.0 μm, 7.5 μm, 12.0 μm) to further validate the scaling law, as shown in Fig. R1. Following this further validated model, we redesigned a structure with the serpentine beam width H increased by 30% (from 1.2 mm to 1.56 mm) and the thickness h_{PI} reduced by 33% (from 7.5 μm to 5.0 μm) to perform approximately the same level of deformation under the same current but in a magnetic field with only ~10% of the original strength. Specifically, we generated 25 mT (11% of 224 mT) by spacing the magnets around three times apart (from 55 mm to 175 mm). which corresponds to a typical field strength generated by a commercial Helmholtz coil (SpinCoil-

7-X, customized, Micro Magnetics, Inc.; coil radius R = 18 mm, number of turns n = 2500, coil current I = 2 A) over a distance of 160 mm. Fig. R1 below shows the experimental results of the redesigned structure maintaining approximately the same Lorentz-force-driven response in the reduced magnetic field of 25 mT. From the standpoint of physical limits, we can further reduce the PI thickness or replace it with low-modulus encapsulation materials so that its contribution to the bending rigidity is negligible. This redesigned structure can maintain the same Lorentz-force-driven response in a minimum possible magnetic field of ~0.2 mT, given our current maximum current density and overall structural size.

We included Fig. R1 as Extended Data Fig. 2 in the revised manuscript. We added detailed discussion of the design principles in Supplementary Note S5.1.

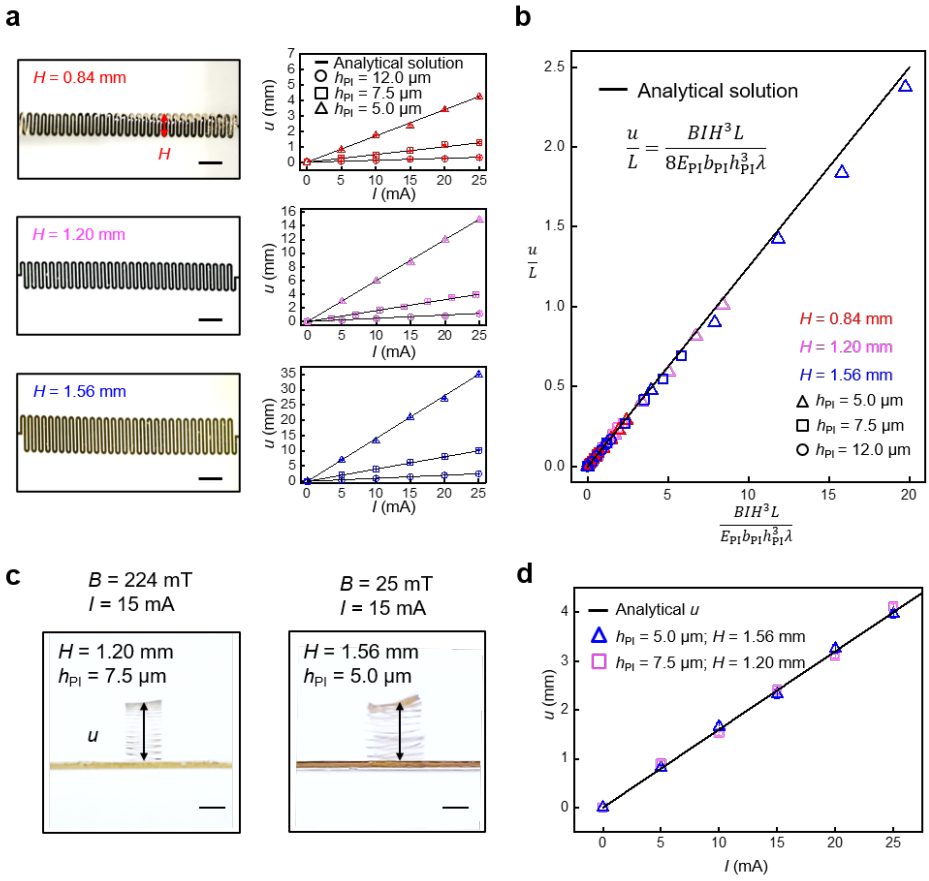

Fig. R1 | Experimental validation of the scaling law using a single serpentine beam. a, Top-view optical images of serpentine beams of the same beam length (L = 11 mm) but different beam widths (H = 0.84 mm, 1.20 mm, 1.56 mm). In a magnetic field of 224 mT, current-controlled experiments show that the electromagnetic responses of the beams with various PI thicknesses (h_{PI} = 5.0 μm, 7.5 μm, 12.0 μm) agree with the analytical solutions. **b,** The experimentally measured electromagnetic responses follow the scaling law predicted by the analytical model. **c,** Side-view optical images of a serpentine beam of the design presented in the main text (H = 1.20 mm, h_{PI} = 7.5 μm) in a magnetic field of 224 mT (left) and a tailored serpentine beam (H = 1.56 mm, h_{PI} = 5.0 μm) in a reduced magnetic field of 25 mT (right). Applying the same current (15 mA) deforms the two beams to the same height (~2.3 mm). **d,** The two beams in (c) exhibit approximately the same current-controlled mechanical behavior. Scale bars, 1 mm.

It is worth noting that this design trades off structural rigidity for large deformation in small magnetic fields. For applications necessitating large work output, we can follow the same engineering guideline to consider stiffer structures and higher currents.

In sum, our systematic experimental, theoretical, and computational studies of the unique electro-magneto-mechanics of our Lorentz-force-driven metasurfaces allow for optimized choices of geometries, layouts, materials, and digital-physical interfaces (voltage/current source, magnetic field strength) for a wide range of application requirements. We added text to highlight this flexibility in the summary paragraph.

Our modifications to the manuscript: We added the above Fig. R1 as Extended Data Fig. 2 to show the additional experimental validation of the scaling law and to demonstrate the widely tunable electromagnetic responses by design. We also reorganized the subpanels in Extended Data Fig. 1 to show the analytical solution and the results of experimental characterization of the Lorentz-force-driven response of a single beam.

On page 4, line 85, we added and revised the text to refer to the design guideline for a tunable electromagnetic response "An analytical model validated by experiment can be used to guide design choices for a tunable electromagnetic response in a broad range of magnetic field strengths (*e.g.*, B reduced to 25 mT; see Extended Data Fig. 2 and Supplementary Note S3.1)."

On page 5, line 102, we added the text to refer to the additional experimental validation of the scaling law "The analytical model and the FEA studies, together with experimental validations, provide a scaling law of the coefficients as $C_{ij} \sim (BLH^2 b_{\mathrm{Au}} h_{\mathrm{Au}})/(E_{\mathrm{PI}} b_{\mathrm{PI}} h_{\mathrm{PI}}^3 \rho_{\mathrm{Au}})$ (H–serpentine beam width, E_{PI}–PI Young's modulus, ρ_{Au}–Au electrical conductivity; see Supplementary Figs. 8 and 9, Supplementary Notes S3.2 and S3.3, for details)."

On page 11, line 259, in the concluding paragraph, we modified the text to highlight the compatibility of our system with different design parameters for wide range of application requirements, as follows "The current modular platform demonstration invites higher levels of integration to embed functional materials and components into the morphing matter, to support on-board power sources (supercapacitors), sensors (strain gauges), feedback control mechanisms (analogue devices), computational resources (microcontrollers), and wireless communication capabilities (radios)."

On page 5 of the Supplementary Information, in Supplementary Note S3.1, we added a detailed discussion of the design principles to achieve a tailorable electromagnetic response of the metasurface. "As suggested by Eq. (S2), increasing the total serpentine width H or decreasing the PI thickness h_{PI} increases the deformation ($u \propto H^3$, $1/h_{\mathrm{PI}}^3$), thereby providing a design guideline for a tunable electromagnetic response in a broad range of magnetic field strengths. For example, increasing H by 30% and decreasing h_{PI} by 33% enables the serpentine structure to exhibit approximately the same deformation for magnetic field strengths reduced by one order of magnitude, as shown in Extended Data Fig. 2."

On page 9 of the Supplementary Information, in Supplementary Note S5.1, we added description of the experimental details "Extended Data Fig. 2a shows serpentine beam structures of the same length (L =11.0 mm) but different widths (H = 0.84 mm, 1.20 mm, 1.56 mm). Extended Data Fig. 2b shows that, in a magnetic field of 224 mT, the current-controlled mechanical responses of the beams with various thicknesses (h_{PI} = 5.0 μm, 7.5 μm, and 12.0 μm) agree with the analytical predictions (Eq. (S2)). The metasurface presented in the main text adopts the serpentine-beam design with H = 1.20 mm and h_{PI} = 7.5 μm and deforms in a magnetic field of 224 mT. Following the scaling law (Eq. (S2), Extended Data Fig. 1b), a beam with H increased by

a factor of g_H and h_{PI} decreased by a factor g_h can maintain the same Lorentz-driven mechanical response in a magnetic field with strength reduced by a factor of $(1+g_H)^{-3}(1-g_h)^3$. Extended Data Fig. 2c shows that a beam with H = 1.56 mm (increased by 30%) and h_{PI} = 5.0 μm (decreased by 33%) performs the approximately the same level of deformation under the same current in a smaller magnetic field 25 mT (reduced to 11%, generated by spacing the magnets apart from 55 mm to 175 mm). The reduced field strength is comparable to that generated by a commercial Helmholtz coil (SpinCoil-7-X, customized, Micro Magnetics, Inc.; coil radius R = 18 mm, number of turns n = 2500, coil current I = 2 A) over large distance (~160 mm). Based on the physics of the response, by reducing the PI thickness or replacing it with a low-modulus encapsulation material such that its contribution to the bending rigidity is negligible, the magnetic field may be reduced to the extreme of ~0.2 mT for the redesigned structure to maintain the same Lorentz-driven response, given the limit on the electric current and overall structure size."

On page 10, line 251, we modified the text to highlight the flexibility of our system "The platform supports optimized choices of materials, geometries, layouts, control systems, and magnetic setup for specific engineering requirements. Its design flexibility and potential scalability promise a wide, versatile application scenario in wearable techniques, soft robotics, and advanced materials."

Comment 3: I don't know if I would call it "self-morphing" since the morphing is induced by external controls.

Our response: We thank the referee for this comment. We agree that the structure is not self-morphing due to the external controls. We use the term "self-evolving" in the original manuscript to emphasize the concepts of a minimum-model or model-free, closed-loop, self-guided inverse-design process, which, in our opinion, is a key advance in our work. We modified the text in the abstract, in the first place in the main text where "self-evolving" appears, and in the concluding paragraph to clarify this definition.

We agree with the referee's technical point that the structure as presented cannot deform on its own, as neither the power source nor the servo is fully integrated into the materials. We would, however, like to highlight that our demonstration platform promises future directions to enable higher levels of integration for the morphing matter to incorporate functional materials and components for on-board power sources (supercapacitors), sensors (strain gauges), feedback mechanisms (analog devices), computational resources (microcontrollers) and wireless communication (radios). These options are available because our system and the methods for its fabrication are well aligned to those of the semiconductor industry generally, and to those of flexible electronics technologies specifically. In the concluding discussion, we modified the text to highlight current limitations as a modular platform and to describe future directions toward system-level enhancements to enable "self-morphing," free of external controls.

Our modifications to the manuscript: On page 2, line 41, we modified the text in the abstract to "… yields surfaces that can follow a self-evolving inverse design to morph into a wide range of 3-dimensional (3D) target shapes with high precision…"

On page 6, line 143, we modified the text to "The existing limitations motivate the development of sensing feedback for a closed-loop self-evolving inverse-design approach."

On page 10, line 237, we modified the text to “The resulting metasurface can follow a self-evolving inverse design to morph to target shapes without prior knowledge of the underlying physics, or with a model-driven prediction to expedite the evolving process.”

On page 11, line 259, we modified the text to “The current modular platform demonstration invites higher levels of integration to embed functional materials and components into the morphing matter, to support on-board power sources (supercapacitors), sensors (strain gauges), feedback control mechanisms (analogue devices), computational resources (microcontrollers), and wireless communication capabilities (radios).”

On page 11, line 263, we modified the text to “Employing advanced data-driven techniques in the loop, … will enhance the capabilities of self-evolving designs for artificial matter in pursuit of capabilities inspired by those in natural counterparts, …”

Responses to comments of Referee #2

Comments from Referee #2:

Summary Comment: This manuscript proposes a novel metasurface that can dynamically morph its shape by having reprogrammable, distributed Lorentz forces. The proposed metasurface is made up by a mesh of serpentine-shaped beams, and desired Lorentz forces can be generated by controlling the electrical current across the beams under a static magnetic field (~0.2 T). There are two control schemes for the proposed metasurface – the open-loop, model-based actuation method and the closed-loop, experiment-driven actuation method. Some notable features of the proposed metasurface are that it can generate a wide range of 3D shapes with high precision and speed (~0.1 s), and it is also very robust since it can still morph into the desired shapes despite having extrinsic or intrinsic perturbations. Such abilities are unprecedented and I believe that the proposed metasurface is highly desirable across a broad range of applications pertaining to soft robotics, wearable technologies and advanced materials.

Overall, I think that this is an excellent novel work, which demonstrates a significant advancement for shape-(re)programmable soft matter. The manuscript is well-written and there is also sufficient data to support the conclusion of this work. The presented showcases are very impressive too. Here are some suggestions that I hope will be beneficial for the authors:

Our response: We thank the referee for the very positive assessment and helpful suggestions. We carefully addressed the issues listed below, and we revised our manuscript accordingly.

Modification to the manuscript: None.

Comment 1: I believe that the range of shapes which can be generated by the proposed metasurface is dependent on its number of independent input voltages. Specifically, a larger range of shapes should be achievable when there are more independent input voltages for the metasurface. In view of this point, can the authors discuss what is the maximum number of voltage inputs that they can provide for their proposed metasurface based on manufacturing or other constraints? Is it possible to create metasurfaces that have more input voltages than the presented 2x2, 4x4 and 8x8 samples in the future?

Our response: We thank the referee for this insightful comment. It inspires and motivates us to include discussions and examples of means to increase the number of voltage inputs to enhance the range of producible shapes and shape responses.

1) In principle, the number of voltage inputs $4N$ of a proposed $N\times N$ metasurface with fixed size can be increased by reducing the unit-cell size L_N. A single-conductive-layer structure with overall size L ultimately accommodates a maximum of $4L/L_N$ ports at its 1-dimensional boundary. Given L, increasing N will provide higher spatial resolution (Nyquist-Shannon sampling theorem). Advanced manufacturing techniques can support feature sizes (*e.g.*, ribbon widths) of the serpentine beams to be reduced by 1~2 orders of magnitude (Ref. S4 in the revised Supplementary Information), such that L_N can scale down to ~100 μm. Meanwhile, the overall size L can scale up easily as the fabrication process is compatible with the well-developed, wafer-based thin-film

manufacturing technology. For example, a design with L = 100 mm (on a 6' wafer) and L_N = 100 μm can support 4×10^3 voltage inputs (N=10^3).

[S4] Zhao, H.B. *et al*., *Proc. Natl. Acad. Sci. U.S.A.* **118**, e2100077118 (2021).

2) A more space-efficient design using denser lattice geometry can increase the number of controls at the boundary, without changing the overall size L or the unit cell size L_N. Figs. R2a and b show that a hexagonal-lattice structure of approximately the same overall/unit-cell sizes as the 4×4 square-lattice structure accommodates twice more voltage inputs (34 vs. 16 ports). The larger number of voltage inputs enhances the range of target shapes (producible with sufficiently small error), as exemplified in Figs. R2c and d for a representative targeting subspace of 3D surfaces.

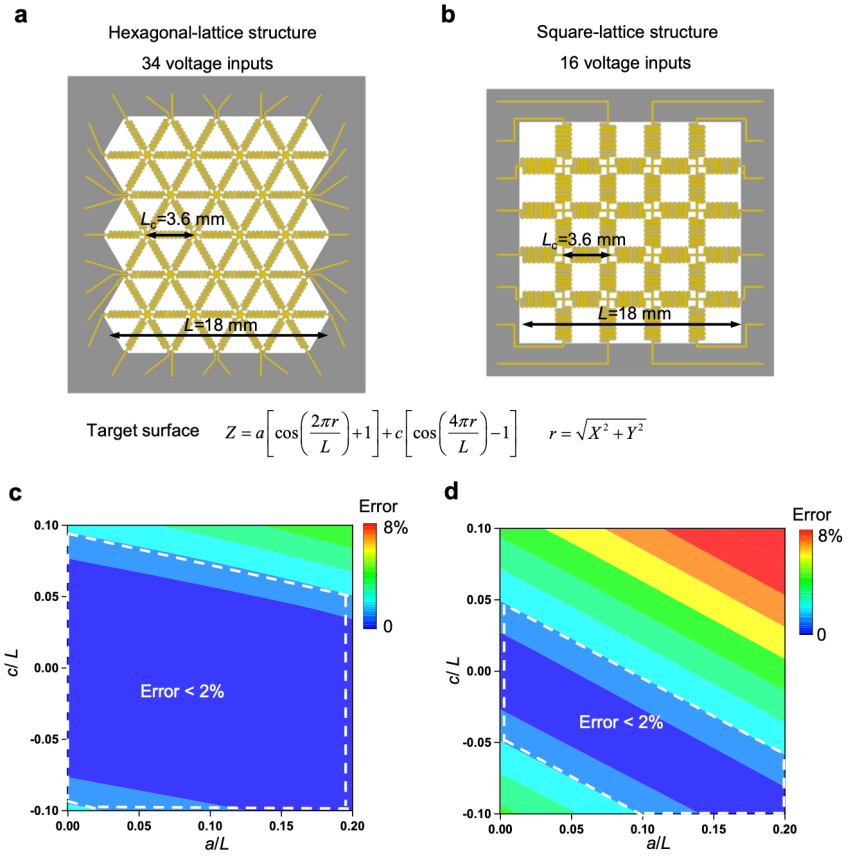

Fig. R2 | A hexagonal-lattice structure to increase the number of voltage inputs. a, Schematic illustration of a hexagonal-lattice structure with 34 voltage-input ports, in comparison with **b**, a square-lattice structure of approximately the same overall and unit-cell sizes, L and L_c. **c,** Error map of the hexagonal structure morphing into a subset of target shapes. A cap of 2% error defines the accessible range of producible shapes. **d,** Error map of the square-lattice structure targeting the same subspace as in (b).

3) Multilayer electrodes can further increase the maximum number of voltage inputs. Integrating hierarchical metasurface structures ($l\times l$ patches, with $l<L$) to increase the length of the control boundaries (from $4L$ to $4L^2/l$) will also boost the number of available input ports.

Our modifications to the manuscript: On page 5, line 118, we added text to refer to the detailed discussion of the scalability of the square-lattice metasurface in Supplementary Information "Fig. 1d shows FEA and experimental results of an inverse-designed, continuous shape morphing of a 4×4 and an 8×8 sample ($L = W = 22.4$ mm; See Supplementary Note S7.1 for detailed discussion of scalability)"

On page 14 of the Supplementary Information, we added Supplementary Note S7.1 "In principle, the number of voltage inputs $4N$ of a $N\times N$ metasurface with fixed size can increase by reducing the unit-cell size L_N. A single-conductive-layer structure with overall size L ultimately accommodates a maximum of $4L/L_N$ ports at its 1-dimensional boundary. Given L, increasing N will provide higher spatial resolution (Nyquist-Shannon sampling theorem). Advanced manufacturing techniques allows feature sizes (*e.g.*, ribbon widths) of the serpentine beams to be reduced by 1~2 orders of magnitude[S4], such that L_N can be scaled down to ~100 μm. Meanwhile, the overall size L can scale up easily as the fabrication process is compatible with the well-developed, wafer-based thin-film manufacturing technology. For example, a design with L = 100 mm (on a 6' wafer) and L_N = 100 μm can support 4×10^3 voltage inputs (N=10^3)."

On page 6, line 134, we added a summary of the suggested ways to enhance the range of shapes, as follows "Increasing the number of control inputs and introducing time-varying magnetic field and field gradient enhance the range of target shapes that can be morphed with sufficient accuracy (see Extended Data Fig. 3, Supplementary Figs. 28, 29, and Supplementary Notes S7 and S12)." and referred the detailed discussion to Supplementary Information.

We added the above Fig. R2 as Supplementary Fig. 28 in the revised manuscript to showcase the larger range of possible shapes with more independent input voltages.

On page 15 of the Supplementary Information, we added Supplementary Note S7.2 "A more space-efficient design of the serpentine network can increase the number of controls, without changing the overall size L or the unit cell size L_N. Supplementary Fig. 28a, b show that a hexagonal-lattice structure of approximately the same overall/unit-cell sizes as the 4×4 square-lattice structure, can accommodate a factor of two increase in voltage inputs (34 vs. 16 ports). The additional voltage inputs enhance the range of target shapes that can be morphed with sufficiently small error, as exemplified in Supplementary Fig. 28c, d for a representative targeting subspace of 3D surfaces."

On page 15 of the Supplementary Information, we added Supplementary Note S7.3 "Multilayer electrodes can further increase the maximum number of voltage inputs. Integrating hierarchical metasurface structures ($l\times l$ patches, with $l<L$) to increase the length of the control boundaries (from $4L$ to $4L^2/l$) will also boost the number of available input ports."

Comment 2: Similar to Point #1, I believe that the range of shapes that can be generated by the metasurface is also dependent on the applied magnetic field. In this study, the applied magnetic field is static and assumed to be uniform due to the configuration of the external magnets. Will it be possible to enhance the range of producible shapes by introducing non-uniform magnetic fields that can also vary with respect to time? I believe that the manuscript can be further strengthened if such discussions can be added.

Our response: Similar to Comment 1, we thank the referee for providing the useful suggestions. It motivates us to include discussions and examples of means to enhance the range of producible shapes and shape responses. We agree with the referee that introducing non-uniform magnetic fields that can also vary with respect to time can further broaden the morphable range. We

performed additional experiments and FEA to investigate two main mechanisms, as discussed below.

(1) A time-dependent, non-uniform magnetic field enables precise spatio-temporal control of the local deformation within a serpentine beam. Figs. R3 below show refined shape-morphing of a single beam under a non-uniform, time-varying magnetic field produced by a small, moving magnet (diameter D = 11.0 mm, thickness h = 5.0 mm, surface field B = 481.6 mT) The asymmetric shape morphing of the beam is not possible in a uniform magnetic field, as the beam always conducts a uniform current.

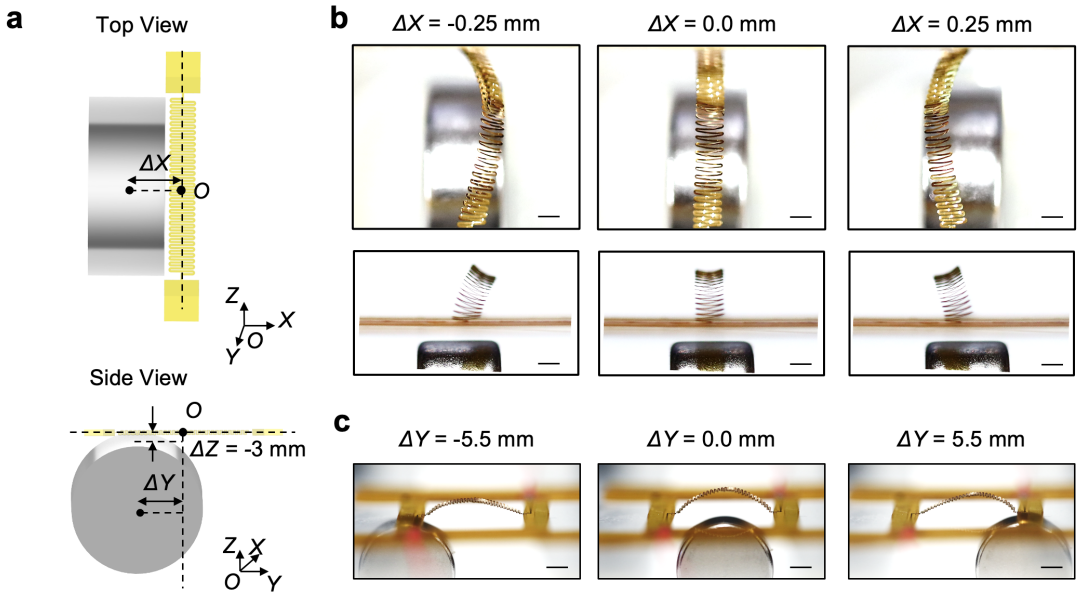

Fig. R3 | Deformation of a single serpentine beam in a time-varying non-uniform magnetic field. a, Schematic illustration of a single serpentine beam in a non-uniform magnetic field generated by a small disk magnet (diameter D = 11.0 mm, thickness h = 5.0 mm, surface field B = 481.6 mT) moving 3-mm below the beam (ΔZ = -3 mm). **b, c,** Optical images of the deformed shapes changing as the position of the magnet changes along X-axis (b, ΔY = 0) and Y-axis (c, ΔX = 0). Scale bars, 1 mm.

(2) A changing field and field gradient can provide extra degrees of spatio-temporal control of the electromagnetic response. Fig. R4a shows a design for a non-uniform magnetic field generated by adding a small magnet 3.0-mm below the center of the 4×4 sample in the existing setup. Measurements of the magnetic flux density shows a superposition of a magnetic field of ~5.0 mm-diameter in the center area to the original field (Fig. R4b). Intuitively, the additional, localized magnetic field facilitates morphing of the metasurface into target shapes with localized deformation around the center of this additional field. Fig. R4c shows experimental results of the 4×4 sample morphing into the same donut-like target shape via experiment-driven self-evolving process in both uniform and non-uniform magnetic field. Both experiment and noise-free simulation show that the metasurface cannot morph into the donut-like shape with sufficiently small error in a uniform magnetic field. In contrast, the non-uniform field environment allows this shape by enhancing the central negative out-of-plane deformation while maintaining the positive displacements around.

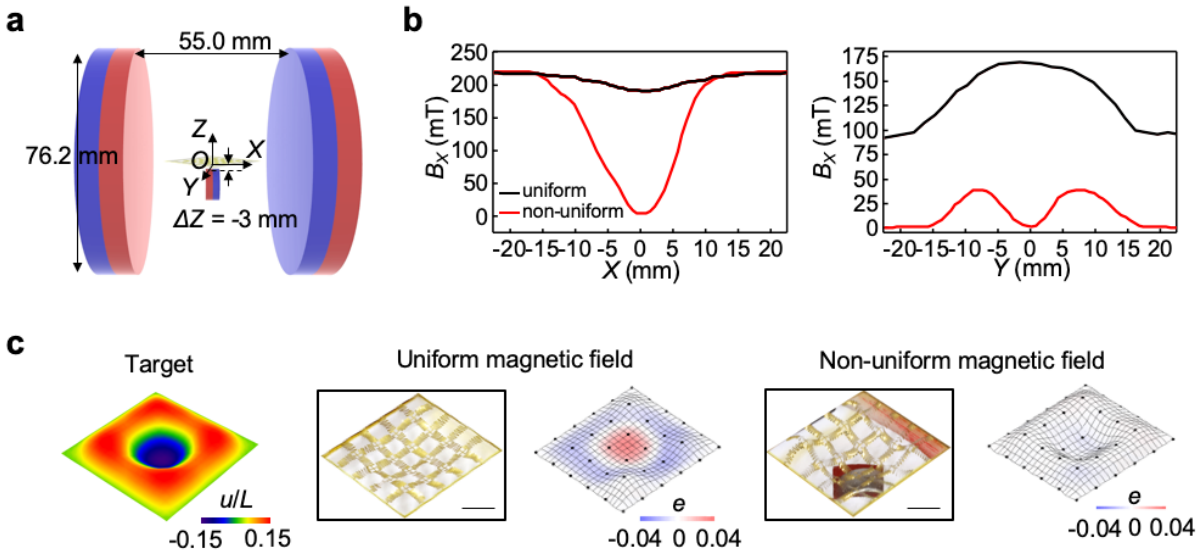

Fig. R4 | A 4×4 sample morphing into a donut-like shape in a non-uniform magnetic field. a, Schematic illustration of a 4×4 sample in a non-uniform magnetic field generated by a pair of large magnets (D = 76.2 mm, h = 12.7 mm, B = 234 mT) and a small magnet (D = 11.0 mm, h = 5.0 mm, B = 481.6 mT) in the middle. **b,** The magnetic flux density of the uniform/non-uniform field measured by a gaussmeter (GMHT201, Apex Magnets) with/without the presence of the small magnet across the center (O) along X-axis (left) and Y-axis (right). **c**, Experimental results of a 4×4 sample morphing into the same donut-like target via the experiment-driven self-evolving process in uniform and non-uniform magnetic field. Optical images of the output results and the 3D reconstructed surfaces superimposed with the error maps. Scale bars, 5 mm.

We also investigated the accessible range in subspaces of 3D surfaces using FEA. We took example Gaussian shapes in the form $Z = c\exp\left(-\frac{X^2+Y^2}{a^2}\right)$ when a is much smaller than the overall structure size L. Fig. R5b shows that the accessible range of these target shapes (bounded by 10% errors) is larger in the localized, non-uniform magnetic field than that in the uniform magnetic field. Fig. R5c shows a similar investigation but in another subspace, with the targeting shapes in the form $Z = a\left[\cos\left(\frac{2\pi(\sqrt{X^2+Y^2})}{L}\right)+1\right]+c[\cos\left(\frac{4\pi(\sqrt{X^2+Y^2})}{L}\right)-1]$. The accessible range reshapes upon the introduction of non-uniform magnetic field, rather than simply expands.

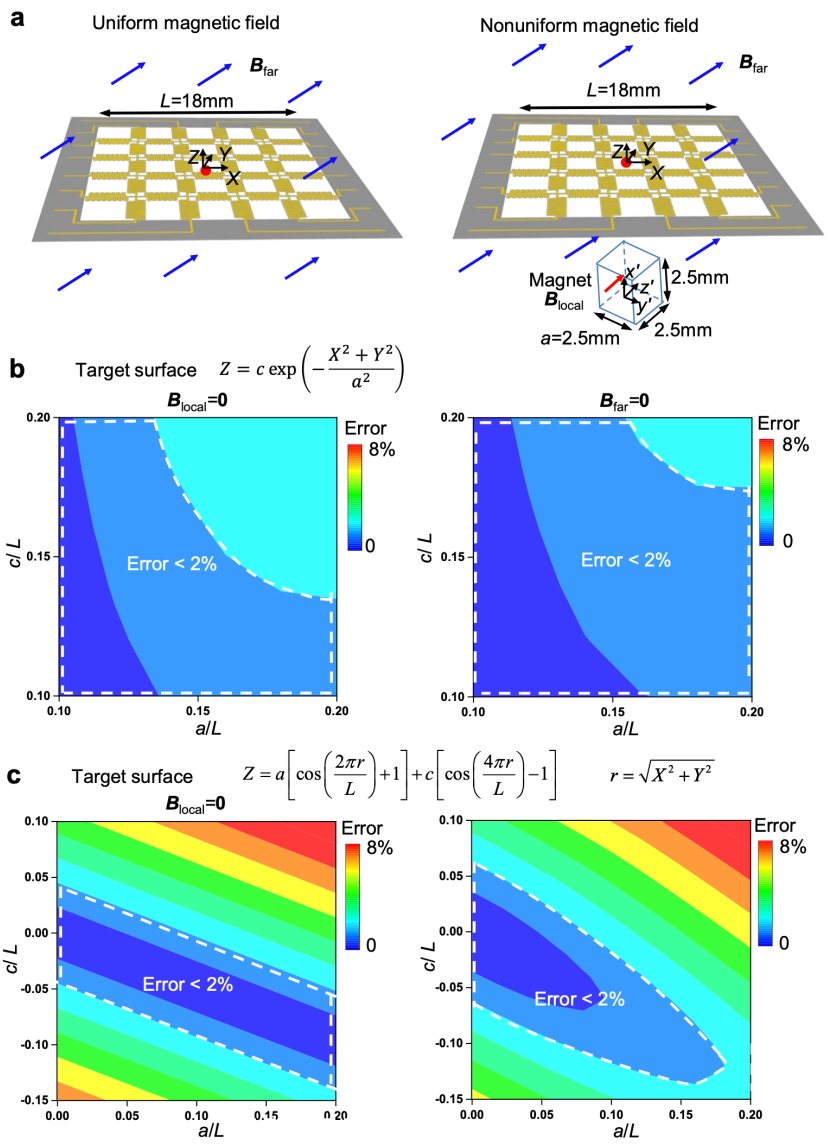

Fig. R5 | FEA investigation of a 4×4 sample morphing into example targeting subspaces in uniform and non-uniform magnetic fields. a, Schematic illustration of a 4×4 mesh structure in a uniform magnetic field $\boldsymbol{B}_{\text{far}}$ (magnitude 224 mT) and a nonuniform magnetic field $\boldsymbol{B}_{\text{far}} + \boldsymbol{B}_{\text{local}}$, where $\boldsymbol{B}_{\text{local}}$ is generated by a small magnet (magnetization M=1.1×10^6 A/m, see Supplementary Note S2.1) below the center of the structure. **b** and **c**, Numerical results of the error between the deformed structure target shapes. In the left panels of (b) and (c), $\boldsymbol{B}_{\text{local}}$ is set to be zero such that the magnetic field is uniform. In the right panel of (b), $\boldsymbol{B}_{\text{far}}$ is set to be zero such that the magnetic field is localized around the center.

In the revised manuscript, we combined and included Figs. R3 and R4 as Extended Data Fig. 3. We added Fig. R5 as Supplementary Fig. 29. We added text in the main text to refer to this additional information. We added Ref. 43 to refer to methods to generate time-varying, non-uniform magnetic fields.

[43] Xu, C. *et al., Adv. Mater.* **33**, 2100170 (2021).

Our modifications to the manuscript: We combined and included Figs. R3 and R4 as Extended Data Fig. 3. We added Fig. R5 as Supplementary Fig. 29.

On page 6, line 134, we added a brief summary of the suggested ways to enhance the range of shapes and referred the detailed discussion to Supplementary Information, as follows "Increasing the number of control inputs and introducing time-varying magnetic fields and field gradients enhance the range of target shapes that can be morphed with sufficient accuracy (see Extended Data Fig. 3, Supplementary Figs. 28, 29, and Supplementary Notes S7.2 and S12)."

Correspondingly, we added text on page 4, line 83 to specify that we used "an approximately uniform magnetic field".

On page 2 of the Supplementary Information, in Supplementary Note S2.1, we added the text about non-uniform magnetic field calculation in FEA "The non-uniform magnetic field generated by the cuboidal magnet (length a, magnetization M along z'- direction in the local $x'y'z'$ coordinate system, see Supplementary Fig.29a) was calculated by the formula below[S3]

$$B_{x'} = \frac{\mu_0 M}{4\pi} \ln\left[\frac{F_2(-x',y',-z')F_2(x',y',z')}{F_2(x',y',-z')F_2(-x',y',z')}\right]$$

$$B_{y'} = \frac{\mu_0 M}{4\pi} \ln\left[\frac{F_2(-y',x',-z')F_2(y',x',z')}{F_2(y',x',-z')F_2(-y',x',z')}\right]$$

$$B_{z'} = -\frac{\mu_0 M}{4\pi} \ln\left[\begin{array}{l} F_1(-x',y',z') + F_1(-x',y',-z') + F_1(-x',-y',z') + F_1(-x',-y',-z') + \\ F_1(x',y',z') + F_1(x',y',-z') + F_1(x',-y',z') + F_1(x',-y',-z') \end{array}\right],$$

with

$$F_1(x',y',z') = \arctan\left[\frac{(x'+a)(y'+a)}{(z'+a)\sqrt{(x'+a)^2+(y'+a)^2+(z'+a)^2}}\right]$$

$$F_2(x',y',z') = \arctan\left[\frac{\sqrt{(x'+a)^2+(y'-a)^2+(z'+a)^2}+a-y'}{\sqrt{(x'+a)^2+(y'+a)^2+(z'+a)^2}-a-y'}\right],$$

and where μ_0 is the magnetic permeability of free space. The magnetization is $M = 1.1\times10^6$ A/m such that the magnetic field at the surface ($x' = y' = 0, z' = a$) is ~400 mT."

[S3] Camacho, J. M. & Sosa, V., *Rev. Mex. fisica E* **59**, 8–17 (2013).

On page 21 of the Supplementary Information, we added Supplementary Note S12 to discuss in details the shape morphing in time-varying, non-uniform magnetic field, as follows,

"Supplementary Note S12: Shape morphing in time-varying, non-uniform magnetic fields

S12.1 Spatio-temporal control of the local deformation within a serpentine beam

A time-dependent, non-uniform magnetic field enables precise spatio-temporal control of the local deformation within a serpentine beam. Extended Data Figs. 3a and b show refined shape-morphing of a single serpentine beam (H = 1.2 mm, h_{PI} = 7.5 μm) in a non-uniform, time-varying magnetic field produced by a small, moving magnet. The small disk-shaped magnet (diameter D = 11.0 mm, thickness h = 5.0 mm, surface field B = 481.6 mT, D73-N52, K&J Magnetics, Inc.), placed 3.0 mm below the center of the beam (ΔZ = -3 mm), generates a localized magnetic field around its instant position. By varying the position of the magnet along the X-axis, the deformed

structure is dragged in the opposite direction of ΔX, as illustrated in Extended Data Fig. 3a. Extended Data Fig. 3b shows a skewed shape of the beam with the peak Z-axis displacement (Z_{max}) shifting along the Y-axis while moving the magnet in the same direction. In a uniform magnetic field, asymmetric shape morphing of a single beam structure is impossible as the beam always conducts a uniform current.

S12.2 4×4 sample morphing into a donut-like shape in a non-uniform magnetic field

A changing field and field gradient can provide extra degrees of spatio-temporal control of the electromagnetic response. Extended Data Fig. 3c shows a design of non-uniform magnetic field generated by adding a small magnet 3.0-mm below the center of the 4×4 sample in the existing setup. Measurements of the magnetic flux density using a gaussmeter (GMHT201, Apex Magnets) shows a superposition of an opposite magnetic field of ~5.0 mm-diameter in the center area to the original field (Extended Data Fig. 3d). Intuitively, the additional, localized magnetic field facilitates morphing of the metasurface into target shapes with localized deformation around the center of this additional field. Extended Data Fig. 3e shows experimental results of the 4×4 sample morphing into the same donut-like target shape via experiment-driven self-evolving process in both uniform and non-uniform magnetic field. Both experiment and noise-free simulation show that the metasurface cannot morph into the donut-like shape with sufficiently small error in the uniform magnetic field. In contrast, the non-uniform field environment allows this shape by enhancing the central negative out-of-plane deformation while maintaining the positive displacements around.

S12.3 FEA and numerical studies on the shape morphing in a non-uniform magnetic field

FEA and numerical studies investigates the accessible range in subspaces of 3D surfaces and demonstrates an enhanced morphing capability due to an alterable, non-uniform magnetic field. Supplementary Fig. 29a shows a design of a nonuniform magnetic field $\boldsymbol{B}_{local} + \boldsymbol{B}_{far}$, where $\boldsymbol{B}_{local}$ is generated by a small magnet (M=1.1×10^6 A/m, see Supplementary Note S2.1) below the center of the 4×4 structure and $\boldsymbol{B}_{far}$ is a uniform magnetic field. To simulate a time-varying magnetic field, $\boldsymbol{B}_{local}$ and $\boldsymbol{B}_{far}$ can be independently turned on or off. Local magnetic field $\boldsymbol{B}_{local}$ facilitates morphing of the metasurface into target shapes with localized deformation around the center of the small magnet. Examples are the Gaussian shapes in the form $Z = c\exp\left(-\frac{X^2+Y^2}{a^2}\right)$ when a is much smaller than the overall structure size L. Supplementary Fig. 29b shows that in a localized magnetic field $\boldsymbol{B}_{local}$ ($\boldsymbol{B}_{far} = \boldsymbol{0}$), the range of the above Gaussian shapes that can be morphed with sufficient accuracy is wider than that in a uniform magnetic field $\boldsymbol{B}_{far}$ ($\boldsymbol{B}_{local} = \boldsymbol{0}$), indicating a better capability for localized shape control. Supplementary Fig. 29c shows a similar investigation but in another targeting subspace, with the targeting shapes in the form, $Z = a\left[\cos\left(\frac{2\pi(\sqrt{X^2+Y^2})}{L}\right)+1\right] + c[\cos\left(\frac{4\pi(\sqrt{X^2+Y^2})}{L}\right)-1]$. Compared to the case in a uniform magnetic field $\boldsymbol{B}_{far}$, the range of target shapes that can be morphed with sufficient accuracy reshapes upon the introduction of a non-uniform magnetic field $\boldsymbol{B}_{local} + \boldsymbol{B}_{far}$, rather than simply expands."

Comment 3: While the proposed metasurface is able to dynamically generate a wide range of shapes, beam bending seems to be its dominant mode of deformation, and I did not observe large tensile or compressive deformations in the experiments. Based on this discussion, I believe that it will be good to explicitly discuss about the available modes of deformation of the proposed metasurface in the manuscript.

Our response: We thank the referee for this comment. The mode of deformation presented in our manuscript is predominantly out-of-plane bending, as the magnetic field is applied in the in-plane direction. In addition, the in-plane stiffness of the serpentine beams in our system is >2 orders of magnitude higher than the out-of-plane stiffness.

In-plane tensile and compressive deformations become appreciable when we introduce an out-of-plane magnetic field for a metasurface (with one side fixed) constructed from beams with sufficiently small in-plane stiffness (~0.02 N), as shown in Fig. R6. We provided FEA estimations for in-plane deformation of the typical serpentine mesh construction presented in the manuscript. We discussed ways to achieve additional modes of deformation for future study. We included Fig. R6 as Supplementary Fig. 34 in the revised manuscript.

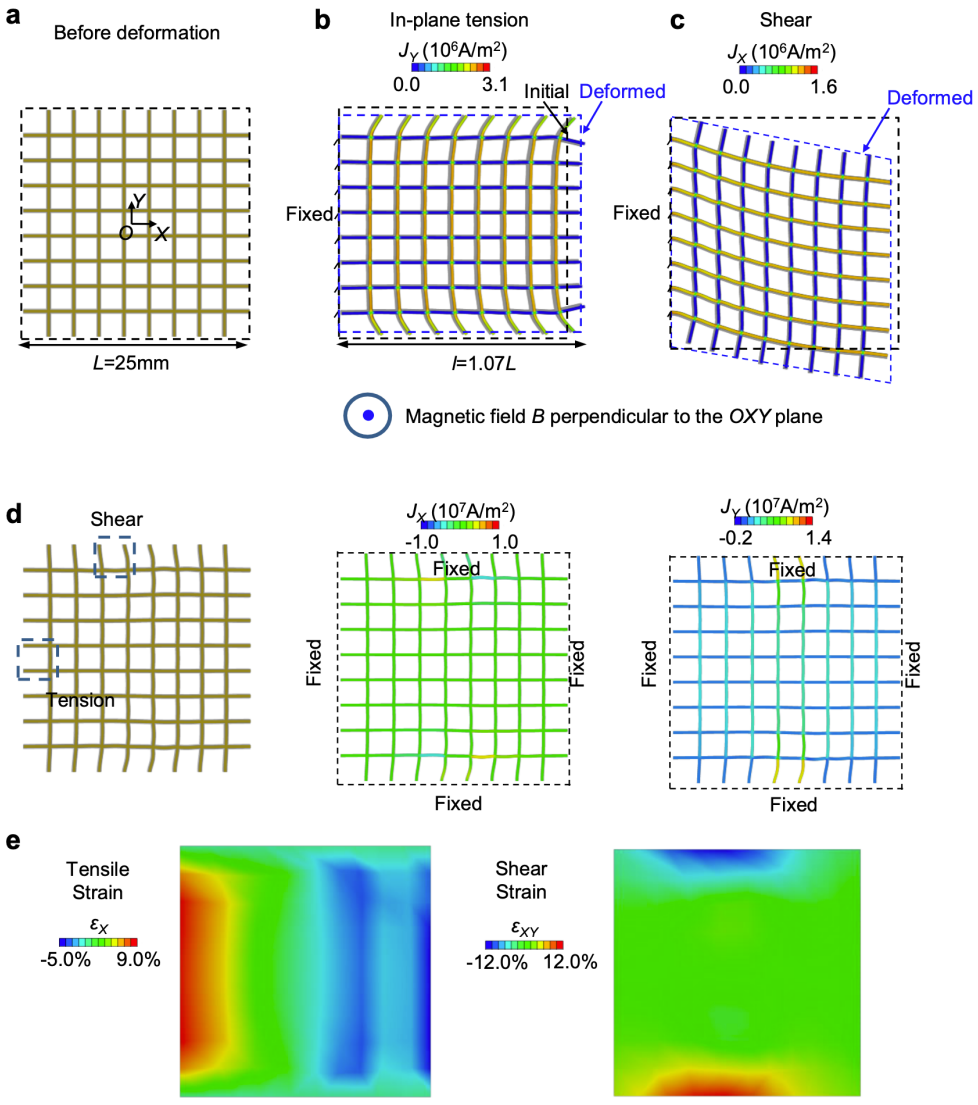

Fig. R6 | Illustration of appreciable in-plane deformations. a, Schematic illustration of a mesh structure with sufficiently small in-plane stiffness (~0.02 N). **b**, FEA result of an in-plane tension deformation of a one-end fixed sample, with the *Y*-component of the current density (J_Y) overlaid (*X*-component $J_X \sim 0$). Applying uniform electric current (0.5A) in the *Y*-direction and a uniform magnetic field (B = 200 mT) perpendicular to the *OXY* plane induces Lorentz forces on the mesh in the *X*-direction. **c**, FEA result of the

shear deformation of a one-end fixed sample induced by a uniform electric current (0.25A) in the *X*-direction. **d**, Complex spatial-varying in-plane deformations of an all-side fixed sample (left) achieved by a non-uniform electric current distribution (middle and right). **e**, contour map of the strain in (d), constructed from the nodal displacements.

Our modifications to the manuscript: We included Fig. R6 as Supplementary Fig. 34.

On Page 4, line 80, we added the text "A tailored serpentine design ensures sufficiently large, fast, and reversible out-of-plane deformation ($u/L\sim30\%$; in-plane deformation <0.01L; response time <0.07 s) of the serpentine beam …"

On page 11, line 257, we added the discussion "Exploring constructions with low in-plane stiffness will enable additional deformation modes of the metasurface (see Supplementary Fig. 34)."

Comment 4: For both the open-loop and the closed-loop actuation methods, a gradient-based algorithm is used to solve an optimization problem that minimizes the error of the system. Are these convex optimization problems? If so, I think that it will be good to state this explicitly in the manuscript as this means that the obtained solution will always be the global solution. If they are not convex optimizations, can the authors discuss about the possibility of getting trapped in a local solution? Although global solvers such as the evolutionary algorithms or particle swarm algorithms are slower than their gradient-based counterparts, will they be helpful in such scenarios?

Our response: We thank the referee for this comment. For the 4×4 and 8×8 morphing structures presented in the manuscript, the optimization problem is theoretically convex as our objective functions (displacement vs. voltage) and constraints (current vs. voltage) are all approximately linear. In the experiment, discreteness in actuation and measurement uncertainties add complexity to the error surface. Extended Data Fig. 6 and Supplementary Note S6.2 (Supplementary Fig. 31 and Supplementary Note S6.2 in the original manuscript) investigated the effect of experimental noise using a model-driven simulator. As a result of this stochasticity, we did observe in our setup, when targeting Shape IV in Extended Data Fig. 5 (Supplementary Fig. 32 in the original manuscript), that the gradient-descent search occasionally failed to reach the desired loss value of $0.005f(\boldsymbol{V}=\boldsymbol{0})$ within 15 iterations. Following the referee's suggestion, we tried a global sover – a pattern search algorithm in model-driven simulation. Fig. R7a shows the optimization of a 4×4 sample morphing into Shape IV, added the typical noise characterized in our experimental setup (Supplementary Fig. 30), the pattern search algorithm requires roughly six times more function evaluations than that of the gradient-based method to reach a loss value of $0.005f(\boldsymbol{V}=\boldsymbol{0})$. When releasing the limit on the number of iterations, both algorithms can find a minimum loss of $0.0005f(\boldsymbol{V}=\boldsymbol{0})$ within 20,000 function evaluations (Fig. R7b). Fig. R7c compares the algorithms in the case with 10 times more noises. While the gradient descent method became trapped in a local solution with a loss of $0.25f(\boldsymbol{V}=\boldsymbol{0})$, the pattern search method could find the same minimum ($0.0005f(\boldsymbol{V}=\boldsymbol{0})$). In sum, as the reviewer suggested, global solvers require more function evaluations compared to gradient-based methods. For a convex problem with minimal noise, the gradient-descent algorithm can provide accurate solutions efficiently. In scenarios where noise is pronounced, or the problem is clearly non-convex, a global solver helps to avoid becoming trapped in a local solution.

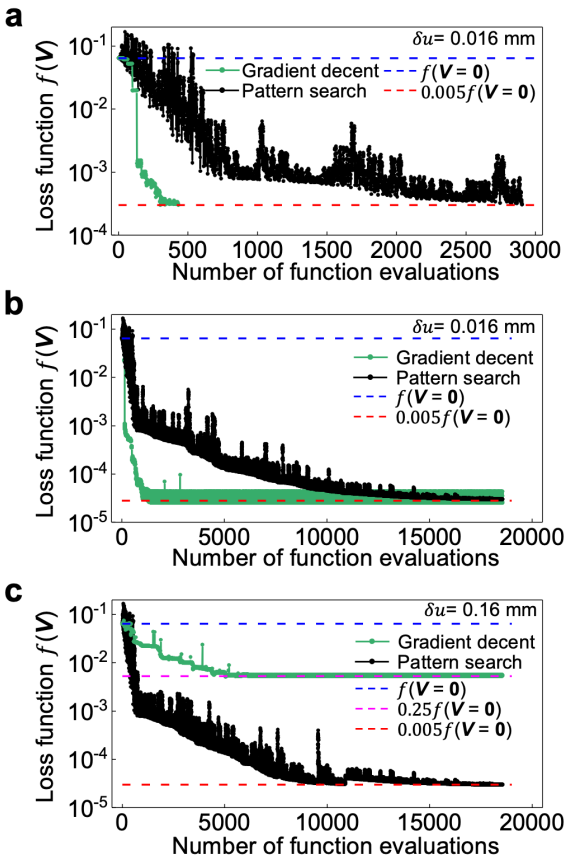

Fig. R7 | Comparison of a global solver with the gradient-based algorithm for a 4×4 sample morphing into Shape IV. a, Typical evolution of the loss function $f(\boldsymbol{V})$ over function evaluations from a model-driven simulation with the objective function subjected to typical experimental noise (δu = 0.016 mm, Supplementary Note S14), targeting a final loss of $0.005f(\boldsymbol{V}=\boldsymbol{0})$. **b,** When releasing the stopping criterion, both algorithms can settle to a minimum loss of $0.0005f(\boldsymbol{V}=\boldsymbol{0})$ within 20,000 function evaluations. **c,** The descent of $f(\boldsymbol{V})$ over function evaluations with pronounced experimental noise (δu = 0.16 mm). The gradient descent method ends with a local solution ($0.25f(\boldsymbol{V}=\boldsymbol{0})$), while the pattern search method finds the same minimum ($0.0005f(\boldsymbol{V}=\boldsymbol{0})$).

The 2×2 mesh structure shown in Fig. 4a and the optical function shown in Figs. 5b–d exhibit nonlinear input-output relationships, such that convexity cannot be guaranteed. However, we do not observe any trapping in local solutions given the objective functions and constraints prescribed in this manuscript.

We included Fig. R7 as Extended Data Figs. 4d–f in the revised manuscript. We added discussions of convexity of our self-evolving problems, as well as the limited performance of the gradient-based optimization process to Supplementary Note S6.2.

Our modifications to the manuscript: We included Fig. R7 as Extended Data Figs. 4d–f in the revised manuscript and referred detailed analysis in Supplementary Note S6.

On page 5, line 109, we added the premise for the general usage of a gradient-based algorithm, as follows "Given a convex problem with linear target functions and constraints, a gradient-descent based algorithm iterates over $\boldsymbol{V}$ to minimize a loss function, $f(\boldsymbol{V}) = \sum_i e_i^2(\boldsymbol{V})$ with a maximum-current constraint (see Methods section 'Optimization algorithm' and Supplementary Note S6 for details).".

On page 7, we moved the discussion of experimental errors "The dominant sources of errors are discreteness in input voltages and uncertainties associated with 3D imaging (Extended Data Fig. 6 and Supplementary Note S14)." from line 164 to line 175. On page 8, line 178, We added the following text to discuss the possible local traps due to experimental noises "Experimental noise also adds complexity to the error function surfaces, and when pronounced, requires global optimization solvers (Extended Data Figs. 4d–f and Supplementary Note S6)."

On page 12 of the Supplementary Information, in Supplementary Note S6.2, we added text to discuss the convexity of our optimization problems "For the 4×4 and 8×8 morphing structures presented in the manuscript, the optimization problems are theoretically convex as the objective functions (displacement vs. voltage) and constraints (current vs. voltage) are all approximately linear. In the experiment, discreteness in actuation and measurement uncertainties add complexity to the error surface. Experimental noise and constraints impose limitations on the performance of the gradient-based optimization process."

On page 13 of the Supplementary Information, in Supplementary Note S6.2, we added the text to provide a detailed investigation of the global solver as the optimization algorithm for the experiment-driven process "As a result of the stochasticity and noise in the experiment, when targeting Shape IV (Extended Data Fig. 5), the gradient-descent search algorithm occasionally fails to reach the desired loss value of $0.005f(\boldsymbol{V}=\boldsymbol{0})$ within 15 iterations. While gradient-based solvers are more efficient for a convex problem with minimal noise, global solvers help to avoid becoming trapped in a local solution when noise is pronounced, or when the problem is clearly non-convex. Extended Data Figs. 4d–f provide an investigation of a typical global solver, the pattern search algorithm, in comparison with the gradient-descent algorithm, using the model-driven simulation of a 4×4 sample morphing into Shape IV (Extended Data Fig. 5). Extended Data Fig. 4d demonstrates the case with the objective function subjected to typical experimental noise (δu = 0.016 mm, Supplementary Note S14). The pattern search algorithm requires around six times more function evaluations than the gradient-based method to reach a loss value of $0.005f(\boldsymbol{V}=\boldsymbol{0})$. When releasing the limit on the number of iterations, both algorithms can find a minimum loss of $0.0005f(\boldsymbol{V}=\boldsymbol{0})$ within 20,000 function evaluations (Extended Data Fig. 4e). Extended Data Fig. 4f compares the algorithms in the case with 10 times more noise (δu = 0.16 mm). While gradient descent method is trapped in a local solution with a loss of $0.25f(\boldsymbol{V}=\boldsymbol{0})$, pattern search method can find the same minimum ($0.0005f(\boldsymbol{V}=\boldsymbol{0})$).

The 2×2 mesh structure shown in Fig. 4a and the optical function shown in Figs. 5b–d exhibit nonlinear input-output relationships, such that convexity cannot be guaranteed. However, given the objective functions and constraints prescribed, the experiment-driven process does not run into any local solutions."

Reviewer Reports on the First Revision:

Referees' comments:

Referee #4 (Remarks to the Author):

The response and revision is thorough and satisfies my technical concerns and better places this work with respect to the literature. The work now looks accurate, with claims supported by the data. My remaining concern is about the ability to actuate at smaller reasonable field strengths, which is a challenge for this class of device. But the authors do fairly state the tradeoff "It is worth noting that this design trades off structural rigidity for large deformation in small magnetic fields". I have some doubts about the utility of the method given the low forces achievable.

Referee #5 (Remarks to the Author):

The authors have responded well in this revision. Overall, I think that this is an excellent work and I would like to recommend publication.

[Redacted]

Responses to comments of Referee #1

Comments from Referee #1:
Summary Comment: The response and revision is thorough and satisfies my technical concerns and better places this work with respect to the literature. The work now looks accurate, with claims supported by the data.

Our response: We appreciate that the referee finds our response and revision satisfying. We thank the referee's previous comments on our work, which helped us better place our work with respect to the literature.

Modification to the manuscript: None.

Comment 1: My remaining concern is about the ability to actuate at smaller reasonable field strengths, which is a challenge for this class of device. But the authors do fairly state the tradeoff "It is worth noting that this design trades off structural rigidity for large deformation in small magnetic fields". I have some doubts about the utility of the method given the low forces achievable.

Our response: We thank the referee for this comment. For applications necessitating large forces, such robotic surfaces, we can follow the engineering guideline provided in the manuscript to optimize choices of materials, geometries, layouts, control systems to adopt stiffer structures and higher currents for large-force utility. On the other hand, the shape-morphing structure of low rigidity finds its potential applications in biomedical engineering for interactions with ultra-soft tissues or bio-interfaces like brains and nerves.

Modification to the manuscript: None. Relevant discussion is included in the ending paragraph.

Responses to comments of Referee #2

Comments from Referee #2:
Summary Comment: The authors have responded well in this revision. Overall, I think that this is an excellent work and I would like to recommend publication.

Our response: We thank the referee for the very positive comment. We are grateful for the referee's previous suggestions that helped us improve this work significantly.

Modification to the manuscript: None.